AEROTHERMAL PERFORMANCE CONSTRAINTS FOR
SMALL RADIUS LEADING EDGES OPERATING AT HYPERVELOCITY

Paul Kolodziej, Jeffrey D. Bull, and Frank S. Milos
Thermal Protection Materials and Systems Branch
NASA Ames Research Center
Moffet Field, CA

Thomas H. Squire
ELORET/Thermosciences Institute
NASA Ames Research Center
Moffet Field, CA

Abstract

Small radius leading edges and nosetips were used to minimize wave drag in early hypervelocity vehicle concepts until further analysis demonstrated that extreme aerothermodynamic heating blunted the available thermal protection system materials. Recent studies indicate that ultra-high temperature composite (UHTC) materials are shape stable at temperatures approaching 3033 K and will be available for use as sharp leading edge components in the near future. Steady-state aerothermal performance constraints for UHTC components are presented in this paper to identify their non-ablating operational capability at altitudes from sea level to 90 km. An integrated design tool was developed to estimate these constraints. The tool couples aerothermodynamic heating with material response using commercial finite element analysis software and is capable of both steady-state and transient analysis. Performance during entry is analyzed by transient thermal analysis along the trajectory. The thermal load condition from the transient thermal analysis is used to estimate thermal stress. Applying the tool to UHTC materials shows that steady-state, non-ablating operation of a HfB_2/SiC (A-7) component is possible at velocities approaching Earth's circular orbital velocity of 7.9 km/s at altitudes approaching 70 km.

Nomenclature

C_T	heat transfer coefficient	(W/cm²-K)
h	enthalpy	(J/kg)
h_D	dissociation enthalpy	(J/kg)
Le	Lewis number = 1.4	
p	pressure	(Pa)
Pr	Prandtl number = 0.71	
q_{cond}	solid heat conduction	(W/cm²)
q_{Fl}	aerothermodynamic heating	(W/cm²)
R_N	radius of wing or nosetip	(m)
$\bar{r}$	normal distance from axis of symmetry	(m)
	to body surface	
T	temperature	(K)
T_r	recovery temperature for heat transfer	(K)
T_{max}	maximum TPS temperature	(K)
U	velocity	(m/s)
x	coordinate in local streamwise direction	(m)
ε_{TH}	total hemispherical emittance	
μ	dynamic viscosity	(kg/m-s)
ρ	density	(kg/m³)
σ	Stefan Boltzman constant	(W/m²-K⁴)

Subscripts

e	boundary layer edge
$t2$	total conditions, behind shock
w	wall
0	stagnation point
∞	freestream
2	behind shock

Superscripts

n	= 0 for nosetip
	= 1 for wing leading edge

Introduction

Because of the aerodynamic advantages, it is important to examine the feasibility of hypervelocity vehicles with sharp leading edges for operation as commercial reusable launch vehicles (RLV's). An important technology for implementing sharp body RLV concepts are shape stable (e.g. non-ablating) sharp leading edge components. Much of the research on these components has focused on developing actively-cooled technologies. Life-cycle costs of actively-cooled leading edges are likely to be of the same order of magnitude as other actively-cooled structures, such as rocket nozzles. Passive, non-ablating, sharp leading edge components with a less complex re-flight certification will inherently have lower life-cycle costs. From this perspective, an

enabling technology for sharp body RLV concepts is the ultra-high temperature ceramic (UHTC) material, such as the zirconium and hafnium diboride composites currently under development by the Thermal Protection Materials and Systems Branch at NASA Ames.[1] UHTCs have a unique combination of mechanical, thermal, and chemical properties that enable the fabrication of very small radius, sharp leading edges, for operation at hypervelocity. To efficiently implement passive, non-ablating, sharp UHTC leading edge components for these new RLV concepts it is necessary to understand: a) their non-ablating operational envelope, and b) their structural thermal behavior. This paper describes an integrated design tool named PERFORM/COSMOS that was developed to provide this capability.

Aerothermal Performance Constraints

Of the many different design approaches that have been used over the past 40 years one of the most useful for quickly assessing the feasibility of a vehicle design with regard to thermal protection system (TPS) capability is the aerothermal performance constraint. This approach uses the properties of the TPS material and the geometry of the leading edge to define a steady-state "non-ablating performance" constraint on the flight envelope. By definition, the surface temperature ($T_{w,0}$) at the stagnation point is constant on this constraint and can be assigned to the maximum non-ablating use temperature of the TPS material ($T_{max,0}$). A surface energy balance at the stagnation point of the leading edge determines the relationship between temperature ($T_{w,0}$), aerothermodynamic heating from the boundary layer fluid ($q_{Fl,0}$), and thermal conduction ($q_{cond,0}$) into the TPS material

$$q_{Fl,0} - q_{cond,0} = \sigma \varepsilon_{TH} T_{w,0}^{\,4}$$
or \hfill (1)
$$T_{w,0} = \left(\left(q_{Fl,0} - q_{cond,0} \right) / \sigma \varepsilon_{TH} \right)^{1/4}$$

For TPS materials with low thermal conductivities $q_{cond,0} << q_{Fl,0}$, and Eq. (1) is simplified to a form commonly known as the equilibrium re-radiated wall temperature boundary condition

$$T_{w,0} = \left(q_{Fl,0} / \sigma \varepsilon_{TH} \right)^{1/4} \hfill (2)$$

For laminar stagnation point heating rates on a hemispherical nose or unswept wing leading edge, the aerothermodynamic heating rate can be determined

from an engineering correlation such as the Fay and Riddell expression

$$q_{Fl} = \frac{0.67}{Pr} \left(\rho_w \mu_w \right)^{0.1} \left(\rho_{l2} \mu_{l2} \right)^{0.4}$$
$$\times \left\{ 1 + \left(Le^{0.52} - 1 \right) \left(h_D / h_{l2} \right) \right\}$$ \hfill (3)
$$\times \left\{ h_{l2} - h_w \right\} \left(\frac{\beta}{2^*} \right)^{1/2}$$

$$\beta = \left(2 \left(p_{l2} - p_\infty \right) / \rho_{l2} \right)^{1/2} / R_N$$

At low velocities $q_{Fl,0}$ is small and $T_{w,0} < T_{max}$, while at high velocities $q_{Fl,0}$ is large and $T_{w,0} > T_{max}$ causing ablation. An algorithm (PERFORM) was developed to iterate on velocity in this manner until $T_{w,0} = T_{max}$ for altitudes from 0 to 90 km. Rarefied flow effects in the fluid and surface catalycity of the material become important at high altitude and must be accounted for in the analysis. Reference 2 discusses how these effects can be handled.[2]

Two examples of steady-state, non-ablating aerothermal performance constraints are shown in Fig. 1 for a sharp 2D leading edge, or wing component. The constraint neglecting conduction will be discussed first. This component is made from ZrB2/SiC (A-10) with a radius of 0.254 cm and a semi-vertex angle of 5 degrees. Temperature dependent material properties for ZrB2/SiC (A-10) are available in the TPSX database.[3] Aerothermal performance constraints for this component are determined using a single-use temperature of 2861 K. For reference, the trajectory (144141) used to design the Shuttle TPS in the 1970s is also shown in Fig. 1.

As altitude increases the aerothermal performance constraint shifts to higher velocities because of decreasing freestream density. It is useful to examine the component performance at constant altitude. When operated on the left-side of the constraint at lower velocities, the component can be continuously operated without ablation. On the right-side of the constraint at higher velocities, operation is possible but ablation begins to blunt the leading edge. It is important to recognize that transient operation on the right-side of the constraint is possible for short duration. Aerothermal performance constraints neglecting conduction have been used in earlier studies of sharp leading edges for hypersonic vehicles.[4]

Because UHTC materials are good thermal conductors at high including the effect of thermal conduction significantly alters the aerothermal performance constraint. The base of the component where it attaches to the airframe is modeled as an adiabatic boundary condition to simulate a worst case

scenario. As expected, solid conduction cools the stagnation point and the aerothermal performance constraint shifts to higher velocities as shown in Fig. 1. This ZrB2/SiC (A-10) component is capable of steady-state operation without ablation at velocities approaching Earth's circular orbital velocity of 7.9 km/s at altitudes approaching 77 km.

The wing of the Space Shuttle Orbiter was designed with a radius of approximately 30 cm for non-ablating operation along the 144141 trajectory. Between 77 and 65 km the 144141 trajectory and the aerothermal performance constraint with conduction practically coincide, indicating this UHTC component is capable of non-ablating operation during a nominal Shuttle entry. Since drag is proportional to area, reducing the leading edge radius from 30 to 0.245 cm reduces the leading edge area by a factor of 122 for identical wing spans. Minimizing this area significantly reduces the pressure drag associated with the leading edge. Although estimating the total drag on wing components is more complicated, this comparison indicates the potential for minimizing pressure drag by utilizing sharp leading edges.

Thermal Conduction

Including thermal conduction adds an order of magnitude in complexity to the analysis because of the interaction between the leading edge geometry and the external flow. To maintain simplicity and a focus on the UHTC material, an engineering correlation was used to determine the aerothermodynamic heating downstream of the stagnation point. For simple geometries such as axisymmetric cones and wedges at zero angle of attack, the downstream pressure distribution (controlling the aerothermodynamic heating) can be determined from curve fits of existing data.[5,6] The heating distribution around the leading edge is calculated from a correlation developed for these types of pressure gradients.[7]

$$\frac{q_{Fl}}{q_{Fl,0}} = \frac{\bar{r}^n \left[\frac{\rho_e \mu_e}{(\rho_e \mu_e)_0} \right] (u_e/u_\infty)}{\left\{ 2^{n+1} \left(\frac{du_e/u_\infty}{dx} \right)_0 f(x) \right\}^{1/2}} \frac{(h_{t2} - h_w)}{(h_{t2} - h_w)_0}$$ (4)

$$f(x) = \int_0^x \left[\frac{\rho_e \mu_e}{(\rho_e \mu_e)_0} \right] \frac{u_e}{u_\infty} \bar{r}^{2n} dx$$

The pressure distribution is used to construct a table of boundary layer edge properties by an isentropic

expansion from the stagnation point conditions. It is important to account for the effects of dissociating, equilibrium air on these properties by using a suitable thermodynamic algorithm such as ACE.[8]

Commercial finite element analysis software, such as COSMOS, usually provide several methods for specifying the thermal boundary condition at the surface.[9] The T-type convective condition:

$$q_{Fl} = C_T (T_r - T_w)$$ (5)

is used to couple the fluid heat transfer from PERFORM to the material response in COSMOS.[10] Several iterations between PERFORM and COSMOS are required to converge on T_w.

Steady-State Thermal Analysis Benchmark

Comparing engineering correlations to higher fidelity numerical techniques reduces uncertainty and builds confidence. For this reason, the sharp leading edge component described above is identical to one used in previous work examining techniques to couple a hypersonic flow field solver with a multidimensional thermal response model (BLIMPK/COSMOS).[11] To minimize the number of elements an axisymmetric, half-plane geometry is used to represent the component. For comparison, a steady-state thermal analysis was performed with and neglecting conduction at a velocity equivalent to Mach 15 at an altitude of 30.48 km. At these conditions the component operates on the right-side of the aerothermal performance constraints shown in Fig. 1 and should exceed the maximum use temperature of 2861 K.

Figure 2 compares the surface temperature profiles from PERFORM/COSMOS and BLIMPK/COSMOS neglecting conduction. Although good agreement occurs near the stagnation point, the temperature of the wedge aft-body is about 130 K lower. Similar results are shown in Fig. 3 for surface temperature profiles with conduction. Again, there is good agreement near the stagnation point while the temperature of the wedge aft-body is lower. The discrepancy between the two methods may be due to differences in the downstream pressure profiles.

Good agreement near the stagnation point indicates that the aerothermal performance constraints shown in Fig. 1 accurately represent the non-ablating, steady-state operational limits of the component. The lower downstream temperature profile from PERFORM/COSMOS has a negligible effect on the stagnation point, but may become important when

designing an attachment between the component and the airframe.

Transient Thermal Analysis Benchmark

In the design of reusable, sharp UHTC leading edge components for hypervelocity flight there are two thermal modes of failure to be addressed. The first is failure by ablation, or melting of the surface, which in severe cases causes a shape change that may gradually affect the aerodynamics. The second is failure by thermal stress fracture, which may abruptly affect the aerodynamics and perturbs the vehicle motion. Because of the high cost of repairing or replacing these components, reusable designs must be capable of nominal performance without failure over a 50 mission life-cycle under normal operations.

Initial ablation occurs when the stagnation point of the leading edge exceeds the single-use temperature of the UHTC material. With a few modifications, the PERFORM/COSMOS integrated design tool can also be used to perform a transient thermal analysis along the trajectory to estimate when this occurs. To build confidence, a comparison was performed between PERFORM/COSMOS and one of the established analysis tools for nosetip thermal response named ASC.[12]

The component used in this comparison is made from a HfB$_2$/SiC (A-7) nosetip with a radius of 0.358 cm and a semi-vertex angle of 5.25 degrees. From arcjet tests, the maximum single-use temperature of HfB$_2$/SiC (A-7) has been estimated to be approximately 3033 K. A conical frustum made from ZrB$_2$/SiC (A-10) interfaces the nosetip to the support structure as shown in Fig. 4. The back wall is adiabatic and the temperature dependent material properties are from the TPSX database. In previous work (see Ref. 1), this component was fabricated and successfully tested in an arcjet at a stagnation point temperature of 3033 K. Because of this successful experience it was used as a preliminary design in the development of a nosetip for the SHARP-B01 flight demonstration. SHARP-B01 is the first hypervelocity flight demonstration of a UHTC leading edge component.[13]

In a transient thermal analysis both initial conditions and time dependent boundary conditions must be specified. For typical entry trajectories, the component is cold soaked during exo-atmospheric flight to a uniform initial temperature, and the transient boundary conditions correspond to the time, altitude, and velocity of the trajectory. In this case, the initial temperature is 233.3 K and the boundary conditions correspond to a nominal trajectory for a ballistic reentry vehicle (RV). Although rarefied flow

phenomena and surface catalycity effects on aerothermodynamic heating of sharp leading edges at high altitude are important, this comparison was done using only continuum, fully catalytic heating for simplicity.

Stagnation point temperatures from PERFORM/COSMOS and ASC are shown in Fig. 5 as a function of altitude. At temperatures greater than 3033 K ablation occurs and the analysis terminates. The size of the discrete time step in the transient boundary condition causes a small overshoot above 3033 K. Temperatures from PERFORM/COSMOS are greater than ASC for the entire altitude range. Because of the higher aerothermodynamic heating, PERFORM/COSMOS terminates at 55.8 km, while ASC terminates at 50.7 km. The discrepancy between these results should be addressed by performing a comparison to a high fidelity benchmark consisting of a direct simulation Monte Carlo (DSMC) method coupled to a material thermal response model such as COSMOS. Estimates of q_{Fl} from DSMC methods are useful for comparison to estimates of q_{Fl} from engineering correlations at high altitude, where rarefied flow effects are important.

Surface temperature profiles from both solvers are shown in Fig. 6 at their respective termination altitudes. As expected, the surface temperature profile from PERFORM/COSMOS is greater than ASC because it terminated with a higher stagnation point temperature. Downstream of the stagnation point both temperature profiles decrease in a similar manner. The maximum discrepancy occurs at the tangent point between the hemispherical nose and the conical frustum where the temperature from PERFORM/COSMOS is approximately 230 K greater than ASC.

Figure 7 compares the transient thermal analysis of this component with the corresponding non-ablating, steady-state aerothermal performance constraint for 3033 K. This HfB$_2$/SiC (A-7) component is capable of steady-state operation without ablation at velocities approaching Earth's circular orbital velocity of 7.9 km/s at altitudes approaching 70 km. This is approximately 7 km lower in altitude than the constraint for the ZrB$_2$/SiC (A-10) component discussed earlier. At 64.5 km the transient analysis crosses the constraint with a stagnation point temperature of 2225 K. The temperature continues to increase during descent until ablation occurs at 55.8 km, approximately 8.7 km after crossing the constraint. This analysis demonstrates the capability for short time operation without ablation on the right-side of the constraint.

Transient Thermal Stress Analysis

Although operating along the aerothermal performance constraint eliminates failure by ablation it is important to recognize that failure by thermal stress fracture may still occur. Rapid, transient heating causes large temperature gradients along the longitudinal axis of the sharp UHTC leading edge component as shown in Fig. 6. As the temperature increases during entry the UHTC material undergoes a multi-dimensional thermal expansion creating internal stress. The resultant stress levels cause failure when the appropriate failure criteria is exceeded. It is important to recognize that the abrupt, step increase in heating experienced by components tested in arcjet facilities is a worst case scenario. For this reason, arcjet facilities are effective in discerning failure by thermal stress fracture. However analyzing this behavior is difficult because of the large uncertainty in the flow environment of arcjet facilities. With a few modifications, the PERFORM/COSMOS integrated design tool can also be used to perform a transient thermal stress analysis of a component operating along a trajectory.

The first step in performing a transient, thermal stress analysis is to determine the thermal load condition resulting from the transient heating along a trajectory. In PERFORM/COSMOS, the thermal load condition is stored by the final step in the transient thermal analysis. By simply terminating the transient thermal analysis at the appropriate time, a thermal load condition can be stored from any point along a trajectory. The thermal load condition that corresponds to the temperature profile shown in Fig. 6 is used here for consistency.

The second step specifies the boundary conditions that are assigned to constrain the displacement caused by thermal expansion and attachment. For this axisymmetric, half-plane geometry the nodes along the longitudinal axis are constrained to displacement along this axis. As a simple attachment, a single node on the longitudinal axis at the back wall is constrained to zero displacement in all directions. In the final step, COSMOS is configured in the normal manner for a static and linear stress analysis with a thermal load condition.

Figure 8 shows the Von Mises element stresses in the sharp UHTC leading edge component caused by thermal expansion. A maximum stress of 126.2 MPa occurs at the surface of the HfB_2/SiC (A-7) slightly behind the tangent point of the cone and hemisphere. Centered on the axis at approximately the same longitudinal distance is another region of high stress with a maximum of approximately 110.3 MPa.

Directly behind this region is an example of the stress caused at an interface between two materials with different thermal expansion coefficients. As expected, stress decreases with increasing distance from the stagnation point where temperature and its gradient are lower. Stress in the cooler ZrB_2/SiC (A-10) is less than 0.8 MPa.

In the simplest evaluation, failure by thermal stress fracture may occur where the stress exceeds the failure criteria. For UHTC components, it is important to recognize that there is a large uncertainty in using this simple evaluation because it is difficult to accurately measure the physical properties of high temperature materials. Historically, this uncertainty has been managed by designers of thermal protection systems through an iterative process involving the fabrication and testing of components to failure. Eventually the material property measurements, analysis capability, and component testing converge to provide a consistent methodology for cost-effective implementation. From this perspective, these stress levels currently serve as useful guidelines in the design of UHTC components.

Conclusions

By analysis of ground facility measurements and flight demonstrations of sharp UHTC leading edge components it will eventually be possible to accurately identify the appropriate non-ablating aerothermal performance constraints for RLV operations. An integrated design tool named PERFORM/COSMOS was developed to provide preliminary estimates of these constraints to designers of hypervelocity vehicles. In addition, this tool is capable of transient thermal analysis along entry trajectories. The thermal load condition from this transient analysis may be used to estimate stress levels in UHTC components. This tool was used in analyzing a preliminary design of the UHTC nosetip for the SHARP-B01 flight demonstration.

Acknowledgment

References

[1] Bull, J. D., Rasky, D. J., Tran, H. K., and Balter-Peterson, A., "Material Response of Diboride Matrix Composites to Low Pressure Simulated Hypersonic Flows," NASA CP-3235 Part 2, May 1994, pp 653-673.

[2] Kolodziej, P., "Aerothermal Performance Constraints for Hypervelocity Small Radius Unswept Leading Edges and Nosetips," NASA TM 112204, July 1997.

[3] Squire, T. H., Milos, F. S., Hartlieb, G. C., and Rasky, D. J., "TPSX: Thermal Protection Systems Expert and Material Property Database," Proceedings of the Fourth International Conference on Composites Engineering, Ed. David Hui, July 1997, pp 937-938.

[4] Hill, M. L., "Materials for Small Radius Leading Edges for Hypersonic Vehicles," J. of Spacecraft and Rockets, Vol. 5, No. 1, Jan. 1968, pp. 55-61.

[5] Cleary, J. W., "Theoretical Aerodynamic Characteristics of Sharp and Circularly Blunt-Wedge Airfoils, " NASA TR R-202, July 1964.

[6] Cleary, J. W., "An Experimental and Theoretical Investigation of the Pressure Distribution and Flow Fields of Blunted Cones at Hypersonic Mach Numbers," NASA TN D-2969, Aug. 1965.

[7] Marvin, J. G. and Sinclair, A. R., "Convective Heating in Regions of Large Favorable Pressure Gradient," AIAA Journal, Vol. 5, No. 11, Nov. 1967, p.1940-1948.

[8] Acurex Corp., "User's Manual Aerotherm Chemical Equilibrium Computer Program (ACE 81)," Acurex Report UM-81-11/ATD, August 1981.

[9] Lashkari, M., "COSMOS/M User Guide, Volume 1," Structural Research and Analysis Corp., Santa Monica, CA, April 1992.

[10] Chen, Y. K., and Milos, F. S., "Solution Strategy for Thermal Response of Nonablating Thermal Protection Systems at Hypersonic Speeds, " AIAA Paper 96-0615, Jan. 1996.

[11] Molvik, G. A., Milos, F. S., Chen, Y.-K., and Squire, T. H., "Computation of High-speed Flow Fields with Multidimensional Solid Heat Conduction," AIAA Paper 95-2116, June 1995.

[12] Rafinejad, D.,Dahm, T. J., Brink, D. F., Abbett, M. J., and Wolf, C. J., "Passive Nosetip Technology (PANT II) Program, Volume 2. Computer User's Manual: ABRES Shape Change Code (ASCC)," Acurex Corp., Rept. SAMSO-TR-77-11, Mountain View, CA, Oct. 1976

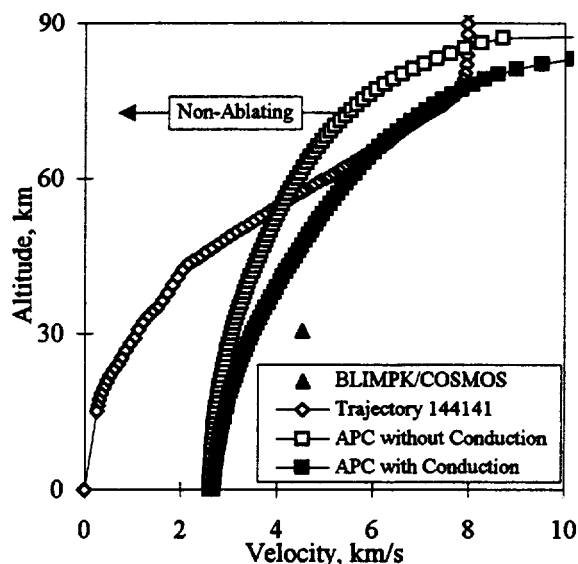[13] http://kauai.arc.nasa.gov/projects/sharp/sharp.html

Figure 1, Steady-state aerothermal performance constraint (APC), with conduction and without conduction for 2D leading edge.
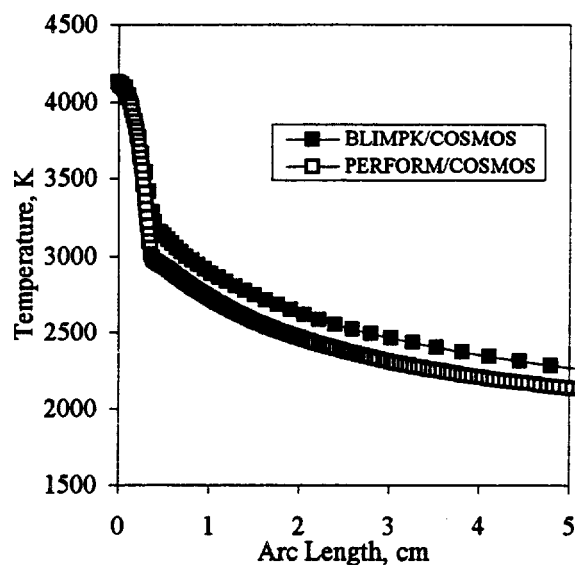

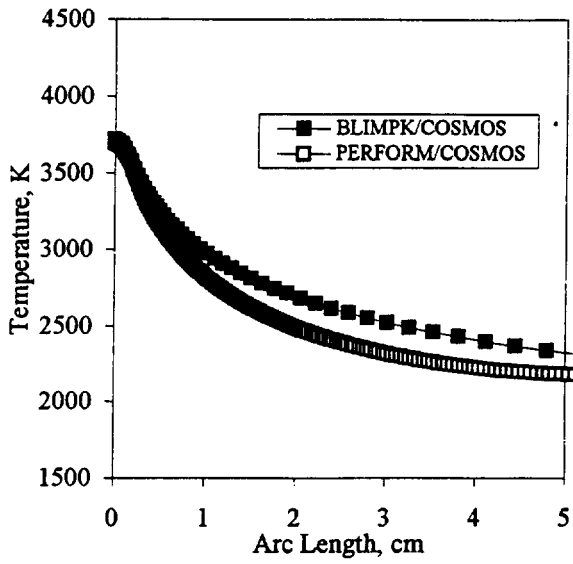Figure 2, Steady-state surface temperature profiles without conduction.

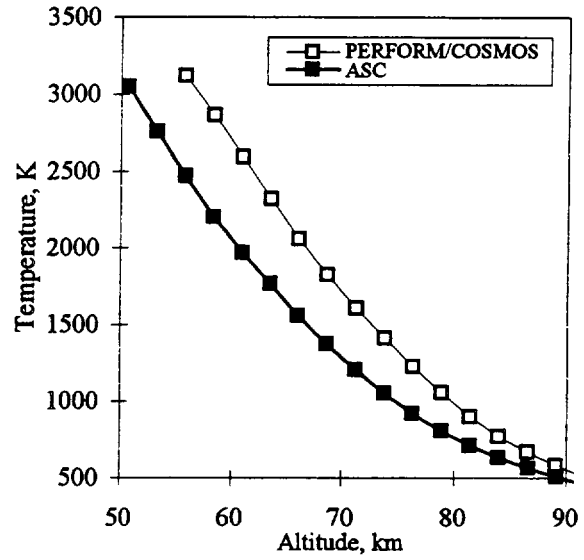Figure 3, Steady-state surface temperature profiles with conduction.

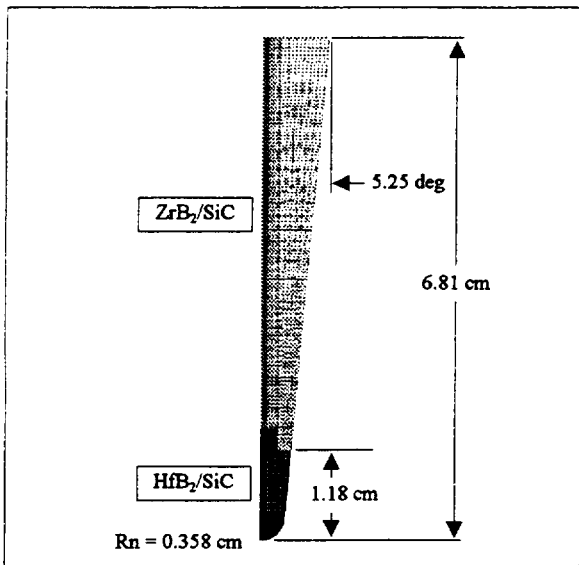Figure 5, Transient stagnation point temperatures.

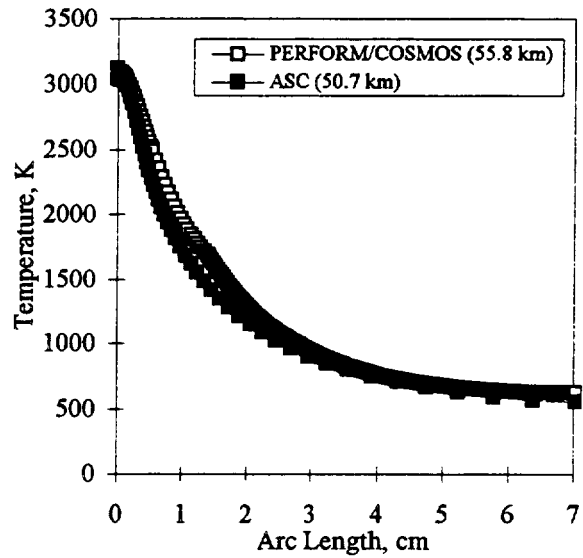Figure 4, Geometry of UHTC leading edge component.

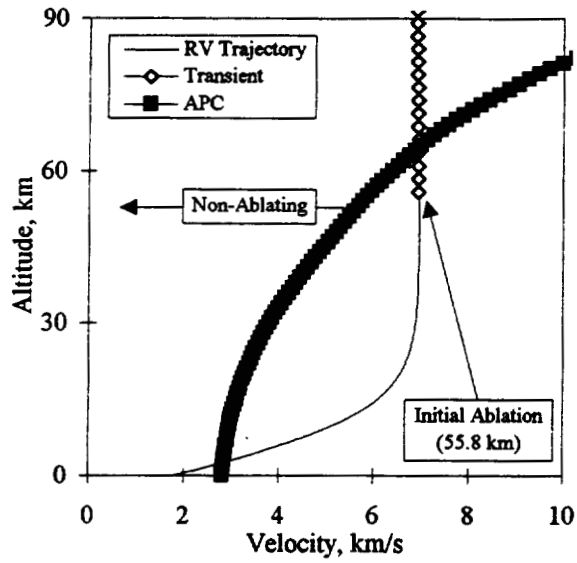Figure 6, Transient surface temperature profiles with conduction.

9-7

Figure 7, Comparison between transient response and steady-state aerothermal performance constraint (APC).
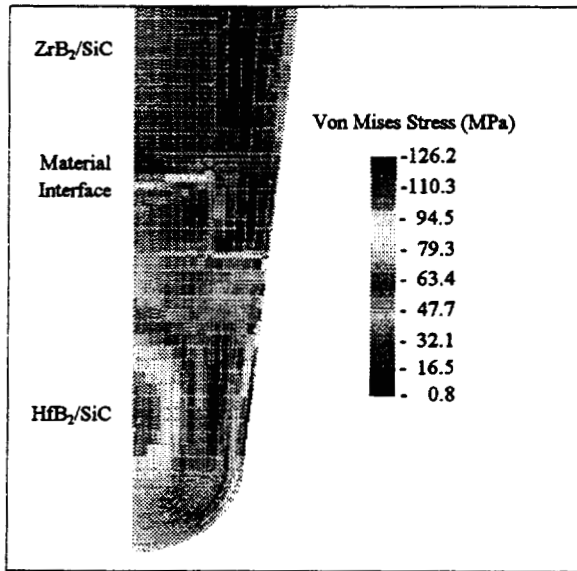

Figure 8, Thermal stress near the stagnation point of the UHTC leading edge component.